Physics in Medicine & Biology

IPEM Institute of Physics and Engineering in Medicine

RECEIVED
23 January 2021

REVISED
23 June 2021

ACCEPTED FOR PUBLICATION
30 June 2021

PUBLISHED
19 July 2021

PAPER

In vivo pulse-echo measurement of apparent broadband attenuation and *Q* factor in cortical bone: a preliminary study

Jean-Gabriel Minonzio[1,2,3], **Chao Han**[1], **Didier Cassereau**[1] and **Quentin Grimal**[1]

[1] Sorbonne Université, INSERM UMR S 1146, CNRS UMR 7371, Laboratoire d'Imagerie Biomédicale, F-75006 Paris, France
[2] Escuela de Ingeniería Informática, Universidad de Valparaíso, Valparaíso 2362735, Chile
[3] Centro de Investigación y Desarrollo en Ingeniería en Salud, Universidad de Valparaíso, Valparaíso, Chile

E-mail: jean-gabriel.minonzio@uv.cl

Keywords: cortical bone, broadband ultrasonic attenuation, quantitative ultrasound, *in vivo* measurement, orthogonal matching pursuit, *Q* factor, sparse reconstruction

Abstract

Quantitative ultrasound (QUS) methods have been introduced to assess cortical bone health at the radius and tibia through the assessment of cortical thickness (Ct.Th), cortical porosity and bulk wave velocities. Ultrasonic attenuation is another QUS parameter which is not currently used. We assessed the feasibility of *in vivo* measurement of ultrasonic attenuation in cortical bone with a broadband transducer with 3.5 MHz center frequency. Echoes from the periosteal and endosteal interfaces were fitted with Gaussian pulses using sparse signal processing. Then, the slope of the broadband ultrasonic attenuation (Ct.nBUA) in cortical bone and quality factor Q_{11}^{-1} were calculated with a parametric approach based on the center-frequency shift. Five human subjects were measured at the one-third distal radius with pulse-echo ultrasound, and reference data was obtained with high-resolution x-ray peripheral computed tomography (Ct.Th and cortical volumetric bone mineral density (Ct.vBMD)). Ct.Th was used in the calculation of Ct.nBUA while Q_{11}^{-1} is obtained solely from ultrasound data. The values of Ct.nBUA (6.7 ± 2.2 dB MHz^{-1}.cm^{-1}) and Q_{11}^{-1} ($8.6 \pm 3.1\%$) were consistent with the literature data and were correlated to Ct.vBMD ($R^2 = 0.92$, $p < 0.01$, RMSE $= 0.56$ dB.MHz^{-1}.cm^{-1}, and $R^2 = 0.93$, $p < 0.01$, RMSE $= 0.76\%$). This preliminary study suggests that the attenuation of an ultrasound signal propagating in cortical bone can be measured *in vivo* at the one-third distal radius and that it provides an information on bone quality as attenuation values were correlated to Ct.vBMD. It remains to ascertain that Ct.nBUA and Q_{11}^{-1} measured here exactly reflect the true (intrinsic) ultrasonic attenuation in cortical bone. Measurement of attenuation may be considered useful for assessing bone health combined with the measurement of Ct.Th, porosity and bulk wave velocities in multimodal cortical bone QUS methods.

1. Introduction

Osteoporosis fracture risk is currently assessed using dual energy x-ray absorptiometry (DXA) in order to assess areal bone mineral density. However, DXA has strong limitations, in particular it lacks sensitivity (Briot *et al* 2013, Siris 2004) and is not appropriate to monitor cortical bone (Choksi *et al* 2018). Cortical bone, the dense tissue that forms the outer shells of the bones, represents about 80% of the human skeleton mass and plays an important role in skeletal mechanical stability (Holzer *et al* 2009, Zebaze *et al* 2010, Bala *et al* 2014). Aging and bone pathologies are associated with cortical thinning (Nishiyama *et al* 2010) and weakening of the bone material mechanical quality reflected in an increase of cortical porosity (Ct.Po) (Kral *et al* 2017) or a decrease of cortical volumetric bone mineral density (Ct.vBMD) (Ostertag *et al* 2016, Paranhos Neto *et al* 2019).

Several quantitative ultrasound (QUS) approaches have been introduced to assess cortical bone health at the radius and tibia. Some aim at assessing cortical thickness (Ct.Th) assuming a nominal value of ultrasound velocity using pulse-echo (Karjalainen *et al* 2008), axial transmission (Moilanen 2008), or through transmission

measurements (Sai *et al* 2010). Other approaches are designed for a combined estimation of Ct.Th and Ct.Po or bulk wave velocities using axial transmission measurements of several guided wave modes (Foiret *et al* 2014, Minonzio *et al* 2019) or adaptative pulse-echo imaging with a transducer array (Renaud *et al* 2018, 2020). Ultrasonic attenuation is another QUS parameter that has been exploited for several decades in soft tissues (Mamou and Oelze 2013) and trabecular bone (Langton and Njeh 2008); however, until now, it has received little consideration in cortical bone QUS.

Ex vivo studies on cuboid specimens have established that ultrasonic attenuation of bulk waves in cortical bone is related to mass density (Bernard *et al* 2015) and to Ct.vBMD (Sasso *et al* 2008). Also, simulations have suggested that the scattering of ultrasound by the cavities of the pore network is one important mechanism of attenuation (Yousefian *et al* 2018, 2021, Iori *et al* 2020). It follows that, in addition to ultrasonic velocities measured with QUS approaches (Grimal and Laugier 2019), attenuation could be indicative of the mechanical quality of cortical bone as it is related to Ct.Po and Ct.vBMD.

There has been a few attempts to measure attenuation in *ex vivo* bone specimens. Zheng *et al* (2007) measured in pulse-echo mode a bovine femur specimen and estimated the slope of the frequency-dependent attenuation coefficient (also referred to as 'spectral ratio method') to estimate the so-called cortical normalized broadband ultrasonic attenuation (Ct.nBUA). They later used a parametric approach introduced by Kuc *et al* (1976) which related attenuation to the shift of the center frequency (also referred to as 'peak frequency method') (Zheng *et al* 2009). Dencks *et al* (2008) also used this parametric approach and measured nBUA in proximal femurs in through-transmission. However, these values of nBUA can hardly be interpreted in terms of bulk cortical bone material properties because ultrasound propagated along a complex path through both cortical and trabecular bone. As far as we know, *in vivo* measurements of attenuation in cortical bone have not yet been reported.

The aim of this paper was to assess the feasibility of *in vivo* measurement of attenuation in cortical bone. We have conducted a preliminary study on the radius of five human subjects. Ultrasound echoes stemming from the normal-incidence reflection on the outer (periosteal) and inner (endosteal) cortical bone interfaces were recorded and processed with orthogonal matching pursuit (OMP) to retrieve the time delay, the temporal echo width, and the frequency shift of the center frequency from which Ct.nBUA and the quality factor Q were calculated with a parametric approach (Kuc *et al* 1976). The quality factor is introduced as a quantity related to the dissipation of energy which can be measured without the need for the knowledge of the bulk wave velocity. Ultrasound parameters Ct.nBUA and Q were compared to reference values of Ct.vBMD of each subject which were obtained with high-resolution x-ray peripheral quantitative computed tomography (HR-pQCT). The results are of interest for the development of future multimodal cortical bone QUS approaches estimating bone structural (thickness) and material (porosity, velocities, attenuation) properties for the evaluation of bone health.

2. Method

2.1. Extraction of echoes

The signal received in the pulse-echo ultrasound measurement is modeled as a sum of two Gaussian pulses $s_i(t)$, or Gabor functions, i.e. the product of a Gaussian function with a complex sinusoid (Demirli and Saniie 2001)

$$y(t) = \sum_{i=1}^{2} s_i(t) + n(t) = \sum_{i=1}^{2} A_i \exp\left[-\frac{(t-t_i)^2}{2\sigma_{t_i}^2}\right] \cos[2\pi f_i(t-t_i)] + n(t), \tag{1}$$

where σ_{t_i} is the standard deviation of the temporal Gaussian function, f_i is the central frequency, t_i is the group delay and A_i is the amplitude of ith echo. The error between the model and the measured signal, including noise, is $n(t)$. The first and second echoes correspond to the reflections on the outer (periosteal) and inner (endosteal) bone surfaces, respectively.

For further use, we write the temporal Fourier transform of one echo as

$$S_i(f) = \frac{A_i}{\sqrt{2\pi}\,\sigma_{fi}} \exp\left[-\frac{(f-f_i)^2}{2\sigma_{fi}^2}\right] \exp[-j2\pi f t_i], \tag{2}$$

where the standard deviation of the Gaussian function σ_{f_i} satisfies $2\pi\sigma_{f_i} = 1/\sigma_{t_i}$. The -6 dB frequency bandwidth, or full width at half maximum, is related to σ_{f_i}, and is equal to $2\sqrt{2\ln(2)}\,\sigma_{f_i} \approx 2.35\sigma_{f_i}$.

The echoes are isolated using a sparse signal processing method in the time domain which provides the quantities σ_{t_i}, f_i, t_i, and A_i ($i = 1, 2$). The method is detailed in appendix; shortly, the signal model, given by (1), discretized in time can be represented as

$$\mathbf{y} = \mathbf{D}\mathbf{x} + \mathbf{n}, \tag{3}$$

where $\mathbf{y}$ and $\mathbf{n}$ are $N_t \times 1$ vectors corresponding to the sampling of $y(t)$ and $n(t)$ at N_t discrete time points, respectively. Likewise, $\mathbf{x}$ is a $N_m \times 1$ vector collecting the N_m relative amplitudes of the echoes. In a sparse point of view, only a few elements of this vector are non-zero. Finally, $\mathbf{D}$ is a $N_t \times N_m$ matrix corresponding to the so-called dictionary. Each column $\mathbf{d}(t;\, \sigma_{t_m},\, f_m,\, t_m)$, with $m = 1 \cdots M$, of $\mathbf{D}$ is one of the M Gabor functions discretized at N_t time points, defined by the set of parameters $(\sigma_{t_m},\, f_m,\, t_m)$. For a given measurement $y(t)$, the problem amounts to determine the two non-zero components of $\mathbf{x}$, which indices yield the set of parameters corresponding to the two echoes. This is done by sparse reconstruction with OMP (Tropp and Gilbert 2007). The details of the construction of the dictionary and of the implementation of OMP can be found in appendix.

2.2. Measurement of attenuation: theory

The cortical bone layer is modeled locally as a plate of thickness Ct.Th. We assume that the temporal signals can be decomposed into monochromatic plane waves propagating in bone at normal incidence on the plate surfaces. The complex wavenumber is denoted $(k + i\alpha)$, where α is the imaginary part and is assumed to present a linear attenuation with frequency in cortical bone, i.e. $\alpha = \beta\, f$ (Minonzio *et al* 2011). This linear approximation, or first-order Taylor expansion, is valid around a central frequency f_0 as long as the frequency deviation Δf is narrow, i.e. $\Delta f / f_0 \ll 1$, even if the attenuation variation for larger frequency is not linear (Szabo 1995, Yousefian *et al* 2021). Note that the real part k of the wavenumber is assumed to be frequency independent within the considered bandwidth. With this plane wave model, the modulus of the ratio of the spectra of the two echoes (from the periosteal and endosteal surfaces) is proportional to $\exp(-\beta f\, 2\text{Ct.Th})$ (Zheng *et al* 2009). Note that the ultrasound signal does not need to be corrected for the overlying soft tissues, as we are studying the ratio between endosteal and periosteal echoes. Both echoes are indeed equally affected by the propagation within the soft tissue layer. Thus, the ratio only depends on the propagation inside the cortical bone layer.

Following Kuc (Kuc *et al* 1976), the attenuation coefficient β can be estimated from pulse-echo measurements with a parametric approach from the shift of the center frequency of the Gaussian pulse. Assuming that the central frequency variation $\Delta f = f_1 - f_2$ is small compared to the central frequency (i.e. σ_f remains unchanged), the coefficient β writes (Kuc *et al* 1976, Narayana and Ophir 1983)

$$\beta = \frac{1}{2\text{Ct.Th}} \frac{\Delta f}{\sigma_f^2}, \tag{4}$$

with the frequency in MHz and distance in mm, β is in Np.mm^{-1}.MHz^{-1}. This parametric estimation is well adapted in both transmission (Kuc *et al* 1976) and reflection (Kuc 1984) and has been successfully applied to bone on *ex vivo* specimens in both configurations (Zheng *et al* 2007, 2009, Dencks *et al* 2008). Finally, the cortical broadband ultrasound attenuation in dB.cm^{-1}.MHz^{-1}, is obtained as

$$\text{Ct.nBUA} = 10\frac{20}{\ln(10)}\beta \approx 86.9\beta. \tag{5}$$

The above equations indicate that the experimental determination of nBUA or β requires the knowledge of Ct.Th. This can be obtained from the x-ray computed tomography scan of the bone, or, alternatively, from ultrasound signals as

$$\text{Ct.Th} = v_{11}\frac{\Delta t}{2}, \tag{6}$$

where $\Delta t = t_2 - t_1$, providing the longitudinal bulk wave velocity v_{11} (in mm.μs^{-1}) is known. The index '11' refers to the radial bone direction commonly denoted direction 1 in previous studies (Foiret *et al* 2014, Bernard *et al* 2015). In a first approach, a nominal value of v_{11} may be assumed, i.e. the velocity is supposed to be known and identical for all subjects (Karjalainen *et al* 2008, Grimal and Laugier 2019). Thus, the β coefficient may be rewritten without reference to Ct.Th, using equations (4) and (6), as

$$\beta = 2\frac{\pi}{v_{11}}\frac{\sigma_t}{\Delta t}\frac{\Delta f}{\sigma_f}. \tag{7}$$

The quality factor Q is a dimensionless parameter, classically used to describe the resonance of a resonator, usually defined by the ratio between the central frequency and the frequency bandwidth. High Q values correspond to low attenuation. It is possible to define a quality factor related to bulk wave velocity v_{11} as $Q_{11}^{-1} = \frac{\Im(C_{11})}{\Re(C_{11})}$ (Bernard *et al* 2015), where C_{11} is the complex elastic coefficient related to v_{11}. Interestingly, as we show below, Q_{11}^{-1} does not require knowledge of the bulk wave velocity. In case of weak attenuation, i.e. $Q_{11}^{-1} \ll 1$ or $\alpha \ll k$, which is usually satisfied in cortical bone at low frequency, i.e. less than a few MHz (Bernard *et al* 2015), the quality factors writes

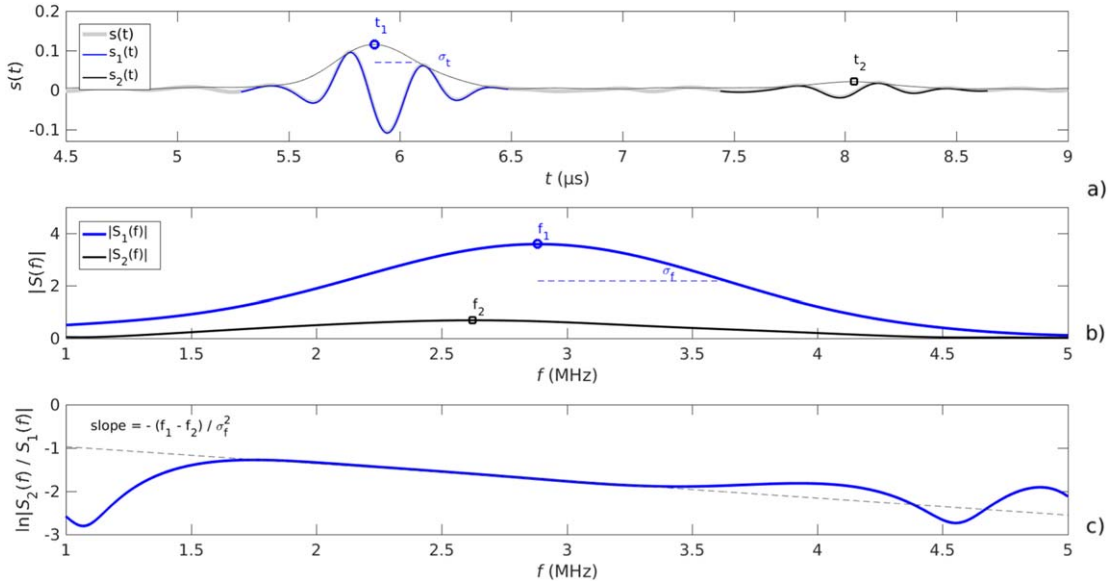

Figure 1. An example of received echoes (for subject number 3) and illustration of the linear frequency dependence of the attenuation coefficient: (a) complete temporal ultrasound signal and retained segments $s_1(t)$ and $s_2(t)$; (b) frequency spectrum of the two echoes and (c) spectrum ratio $\ln(|S_2(f)/S_1(f)|)$ compared with the slope $\Delta f/\sigma_f^2$ obtained with Kuc's formula. The parameters $t_{1,2}$, $f_{1,2}$ and σ_t obtained with OMP in this study are indicated on the figures.

$$Q_{11}^{-1} \approx \frac{2\alpha}{k} \approx \frac{\beta v_{11}}{\pi}. \tag{8}$$

Which can advantageously be rewritten

$$Q_{11}^{-1} \approx \frac{1}{\pi\sigma_f^2}\frac{\Delta f}{\Delta t}, \tag{9}$$

which expression does not depend on the bulk wave velocity v_{11} but only on the parameters Δt, Δf and σ_f which can be extracted from the measured signals. Thus, evaluating Q_{11}^{-1} to measure attenuation could be an advantage as this does not require knowledge of the bulk wave velocity.

2.3. *In vivo* ultrasound measurements

This study has been approved by the ethical committee of the Committees for the protection of persons Sud-Méditerranée. Written informed consent was provided by the five healthy subjects (24–38 years old) recruited in this study. The ultrasound measurements were approximately performed in the one-third distal extremity of the left radius. Precisely, a mark with a pen was done on the upper medial part of the forearm at 7 cm from the radial styloid and the transducer was positioned on this mark. This position exactly corresponded to the center of the region of interest (ROI) scanned with HR-pQCT. A 3.5 MHz center frequency mono element transducer (Olympus V384, 25 mm diameter, –6 dB bandwidth of 2.03 MHz, Webster, TX 77 598, USA) was used. The transducer was connected to a wave pulse/receiver (Olympus 5077PR SQUARE, Waltham, MA 02 453, USA) and an oscilloscope (PicoScope 5000 Series, Picotechnology, Cambridgeshire, United Kingdom) for data acquisition. The sampling frequency was equal to 125 MHz. Ultrasound echoes stemming from the reflection on the outer (periosteal) and inner (endosteal) cortical bone interfaces were recorded. The waveform of the received signal was displayed on the computer screen in real-time. The operator ensured a correct positioning of the probe (perpendicular to interfaces) by slightly moving the probe so as to minimize the time delay between echoes. When a satisfactory position was achieved, the operator started the acquisition of 30 consecutive signals. Note that the ultrasound signal does not need to be corrected for the overlying soft tissues, as we are studying the ratio between endosteal and periosteal echoes.

In order to illustrate the validity of the linear frequency dependence of the attenuation coefficient, a typical example of *in vivo* pulse echo measurement is shown in figure 1. The two separated echoes can be observed on figure 1(a), while the two associated spectra $S_1(f)$ and $S_2(f)$ are shown in figure 1(b). Those spectra were obtained by the temporal Fourier transforms of segments $s_1(t)$ and $s_2(t)$, indicated with thick lines, corresponding to 1.2 μs from each side of the envelop maxima (Karjalainen *et al* 2008). Finally, on figure 1(c), one can observe that the variation of the spectrum ratio $\ln(|S_2(f)/S_1(f)|)$ is in agreement with the slope $\Delta f/\sigma_f^2$

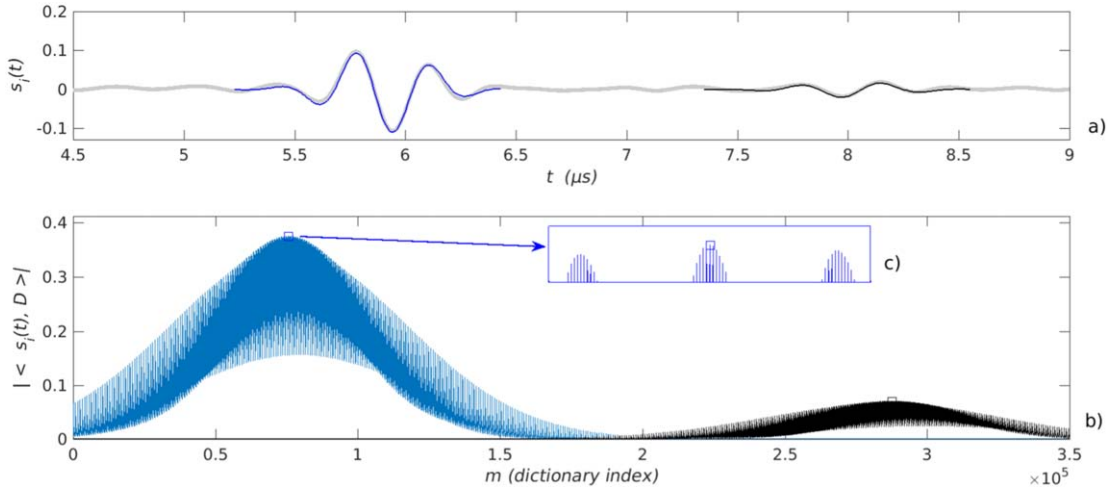

Figure 2. Principle of the evaluation of the parameters (σ_{t_m}, f_m, t_m) of the Gabor functions matching the two echoes using OMP. Original signal $y(t)$ compared with the two reconstructed echoes $s_1(t)$ (blue) and $s_2(t)$ (black) (a) associated with dictionary indices m corresponding to the two largest values of the scalar product between the signal and the dictionary (b). (c): Zoom around the first maximum.

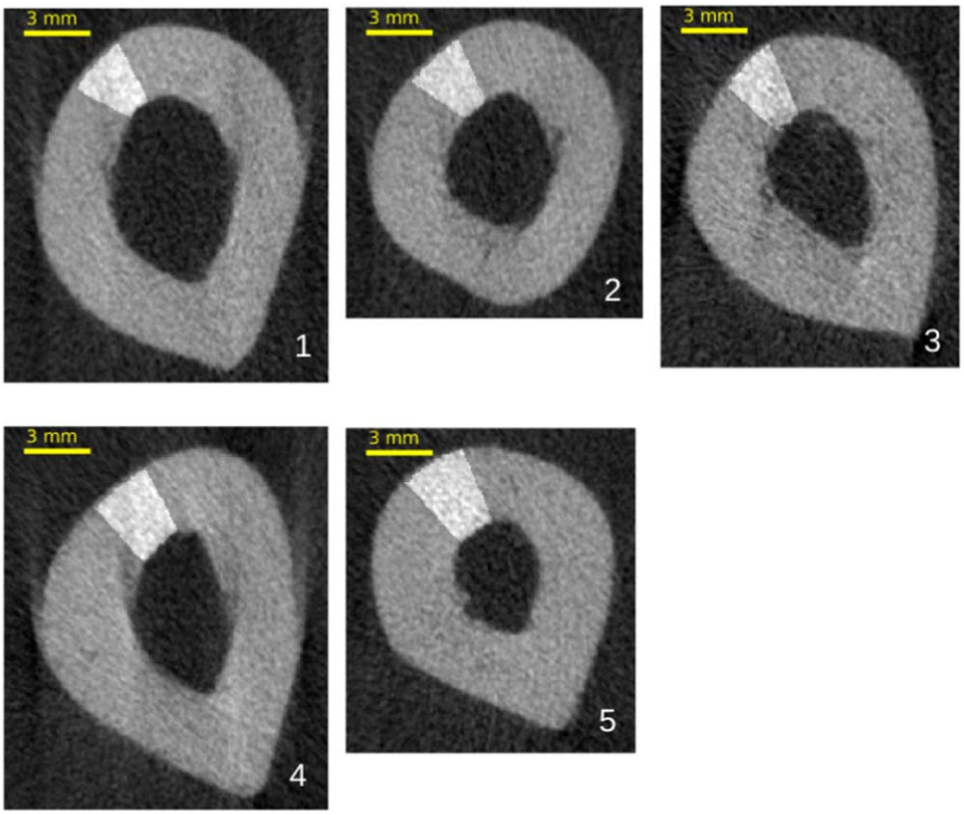

Figure 3. A representative cross-sectional HR-pQCT slice of the radius for each subject. The region of interest corresponding to the ultrasound measurement site is highlighted.

of the linear approximation (Kuc *et al* 1976). Note that the spectral ratio method is based on the slope evaluation, while the peak frequency method is based on Kuc's formula.

Processing of the signal with OMP yields the parameters (σ_{f_1}, f_1, t_1) and (σ_{f_2}, f_2, t_2) of the echoes which were used to calculate Ct.nBUA (equation (5)) using the Ct.Th value obtained from HR-pQCT (see section 2.4) (equation (4)) and Q_{11}^{-1} (equation (9)). The extraction of the parameters (σ_{t_1}, f_1, t_1) and (σ_{t_2}, f_2, t_2) is illustrated on figure 2 using the same signal as for figure 1. It can be observed in figure 2(b) that the retained parameters (best model number m) are associated with the two maxima, for all m, of the scalar product $<s(t)|\mathbf{d}(t; \sigma_{t_m}, f_m, t_m))|>$ between the dictionary and the signal. The maximum of this scalar product can be

Table 1. Ultrasound measurements: Δt is the arrival time difference between the two echoes, Δf is the shift of central frequency, σ_f is related to the frequency bandwidth. The quality factor Q_{11}^{-1} is calculated from these three quantities and Ct.nBUA is calculated using the ultrasound measurements and Ct.Th measured with Ht-pQCT.

Subject No.	Δt (μs)	Δf (MHz)	σ_f (MHz)	Q_{11}^{-1} (%)	Ct.nBUA (dB.MHz^{-1}.cm^{-1})
1	1.67 ± 0.02	0.21 ± 0.15	0.94 ± 0.03	5.1 ± 3.4	3.7 ± 2.5
2	1.75 ± 0.04	0.34 ± 0.13	1.05 ± 0.19	8.4 ± 2.6	6.5 ± 2.2
3	1.70 ± 0.02	0.46 ± 0.07	0.81 ± 0.02	13.5 ± 3.1	9.5 ± 2.3
4	2.14 ± 0.08	0.51 ± 0.11	0.93 ± 0.06	9.1 ± 1.8	7.8 ± 1.7
5	2.32 ± 0.04	0.37 ± 0.16	0.89 ± 0.06	6.8 ± 3.6	5.8 ± 3.1
Mean ± std	1.92 ± 0.30	0.38 ± 0.12	0.92 ± 0.09	8.6 ± 3.1	6.7 ± 2.2

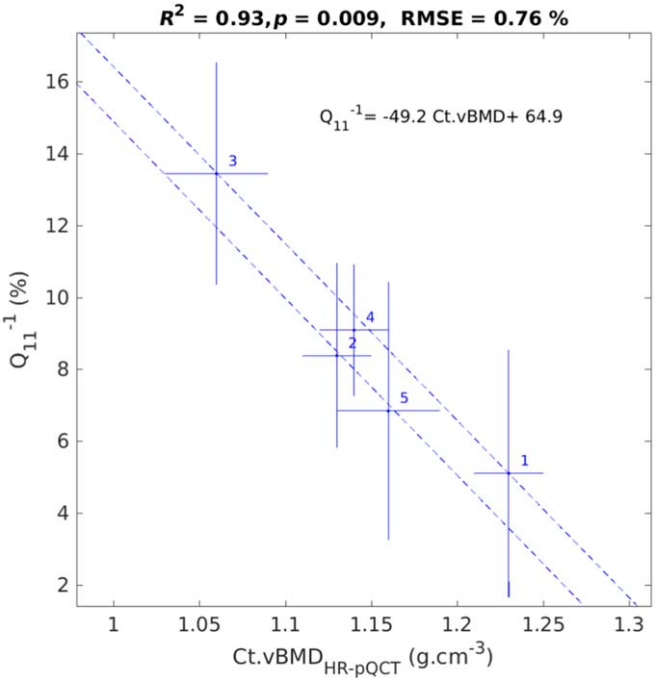

Figure 4. Correlation between quality factor Q_{11}^{-1} obtained by pulse-echo and Ct.vBMD obtained by HR-pQCT.

interpreted as the maximum quality of the signal fit, as the dictionary vectors **d** are normalized. Accordingly, for each subject, we retained the 10 (out of 30) measurements with the highest values in order to remove the poorest measurements corresponding e.g. to a poor alignment of the probe with the bone surface. The final values of nBUA and Q_{11}^{-1}, and their errors, were obtained using the mean and the standard deviation calculated on the 10 retained measurements.

2.4. HR-pQCT

The left radius of each subject was scanned with HR-pQCT (XtremeCT, Scanco Medical, Brüttisellen, Switzerland) using the standard manufacturer *in vivo* acquisition parameters (60 kVp, 1000 mA, 100 ms integration time, voxel size 82 μm). The measurements were approximately performed at the one-third distal radius site. To ensure that HR-pQCT imaging is site-matched with ultrasound measurement, we used an initial large view image allowing to center the scanning windows at 7 cm from the radial styloid corresponding to the ultrasound measurement point. The acquired volume corresponded to 9.02 mm along the bone axis (110 cross-sectional slices). The central slice is illustrated in figure 3 for each subject. The ROI, site-matched with the ultrasound measurement site, is highlighted. Methods used to process the CT data have been previously described in detail (Laib *et al* 1998, Boutroy *et al* 2005, MacNeil and Boyd 2007, Ostertag *et al* 2016). Briefly, cortical limits were determined using a threshold-based algorithm. The threshold used to discriminate cortical bone was set to one-third of the apparent cortical bone density value (Dcort). Ct.Th was calculated for each slice as the mean distance between the periosteal and endosteal contours. Finally, the mean and standard deviation of all slice Ct.Th was retained for each subject. Volumetric bone mineral density of the cortical bone in the ROI (Ct.

Table 2. Cortical thickness (Ct.Th) and volumetric bone mineral density (Ct.vBMD) obtained from HR-pQCT images.

	HR-pQCT	
Subject No.	Ct.Th (mm)	Ct.vBMD (g.cm^{-3})
1	3.11 ± 0.08	1.23 ± 0.02
2	3.13 ± 0.02	1.13 ± 0.02
3	3.28 ± 0.06	1.06 ± 0.03
4	3.43 ± 0.02	1.14 ± 0.02
5	3.79 ± 0.03	1.16 ± 0.03
Mean ± std	3.35 ± 0.28	1.14 ± 0.06

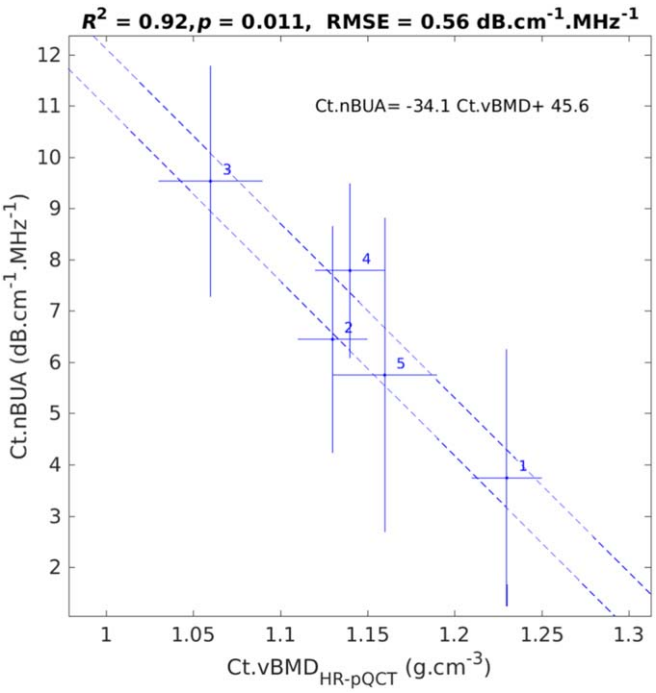

Figure 5. Correlation between Ct.nBUA and Ct.vBMD.

vBMD) was obtained directly from Dcort. The mean and standard deviation of all slice Dcort was retained for each subject.

2.5. Data analysis

The relationships between ultrasound parameters and reference parameters obtained with HR-pQCT were assessed using linear correlations. We report Pearson's correlation coefficient and linear regression equations.

3. Results

The mean and standard deviation, calculated over the ten retained measurements, of the estimated parameters Δt, Δf, σ_f for each subject are reported in table 1. The next to last column corresponds to Q_{11}^{-1} obtained combining previous parameters using equation (9). Finally, values of Ct.Th, Δf and σ_f were used to compute Ct.nBUA according to equations (4) and (5) (last column of table 1). HR-pQCT parameters Ct.Th and Ct.vBMD are reported in table 2.

High correlations were observed between Q_{11}^{-1} and Ct.vBMD, obtained by HR-pQCT ($R^2 = 0.93$, $p < 0.01$, RMSE =0.76%, figure 4) and between Ct.nBUA and Ct.vBMD ($R^2 = 0.92$, $p < 0.01$, RMSE=0.56 dB.MHz^{-1}.cm^{-1}, figure 5). The linear regression equation was Ct.nBUA= $-34.1 \times$ Ct.vBMD $+ 45.6$, where Ct.nBUA is expressed in dB.MHz^{-1}.cm^{-1} and Ct.vBMD in g.cm^{-3}. Likewise, the second linear regression equation was $Q_{11}^{-1} = -49.2 \times$ Ct.vBMD $+ 64.9$, where Q_{11}^{-1} is expressed

Table 4. Normalized broadband ultrasonic attenuation (nBUA) values published in the scientific literature and in this study. Mean values are given, and standard deviation when available.

Reference	Species and skeletal sites	Number of samples	Frequency range or center frequency (MHz)	nBUA (dB MHz^{-1} cm^{-1})
Lakes *et al* (1986)	Bovine femur (*ex vivo*)	1	1–7	~3
Lees and Klopholz (1992)	Bovine femur (*ex vivo*)	4	0–30	~4
Han *et al* (1996)	Bovine femur (*ex vivo*)	5	0.3–0.7	5–12
Zheng *et al* (2007)	Bovine femur (*ex vivo*)	8	2.25	4.91 ± 0.65
Sasso *et al* (2008)	Bovine femur (*ex vivo*)	40	3.5–4.5	4.2 ± 2.4
Talmant *et al* (2019)[a]	Human femur (*ex vivo*)	35	2–8	4.9
This paper	One-third distal radius (*in vivo*)	5	3.5	6.7 ± 2.2

[a] In Talmant *et al* (2019), the reported attenuation normal to the direction of osteons is, at 4 MHz, 3.9 dB.cm^{-1} per percentage of porosity; the value given in the table is calculated for a very moderate porosity of 5% characteristic of the bone of a healthy young adult.

Table 3. Longitudinal bulk wave velocities calculated as $v_{11} = 2\text{Ct.Th}/\Delta t$ using values given in tables 1 and 2.

Subject No.	v_{11} (mm.μs^{-1})
1	3.72 ± 0.14
2	3.58 ± 0.10
3	3.86 ± 0.12
4	3.21 ± 0.14
5	3.27 ± 0.08
Mean ± std	3.53 ± 0.28

in % and Ct.vBMD in g.cm^{-3}. The corresponding longitudinal bulk wave velocities v_{11}, ranging from 3.2 to 3.9 mm.μs^{-1}, are given in table 3 for comparison with other studies.

4. Discussion

This work considered pulse-echo measurements to measure the attenuation of signals from ultrasonic waves propagating in cortical bone at the radius *in vivo*. The two echoes stemming from normal-incidence reflections on the periosteal and endosteal bone surfaces were modeled as the sum of two elementary waveforms (Gabor functions), and the parameters of these waveforms (time delay, central frequency, and frequency bandwidth) were recovered using sparse signal processing (OMP). Attenuation was assessed in two ways: (1) as Ct.nBUA with a parametric method using OMP parameters combined with Ct.Th from HR-pQCT; and (2) as a quality factor Q_{11}^{-1} calculated from OMP parameters only.

The values of Ct.nBUA (6.7 ± 2.2 dB.$MHz.^{-1}$.cm^{-1}) are in the range of the attenuation values reported in the literature on bovine and human femur (table 4). To which extent Ct.nBUA and Q_{11}^{-1} reflect the true (intrinsic) ultrasonic attenuation in cortical bone remains to be investigated. Such quantity can only be evaluated *ex vivo* using dedicated experimental conditions in order to minimize the effect of diffraction and other losses unrelated to attenuation within the tissue.

We found that Ct.nBUA was strongly correlated to Ct.vBMD measured from x-ray attenuation ($R^2 = 0.92$, figure 5). This finding is in line with the *ex vivo* results of Sasso *et al* (2008) who reported a correlation between Ct.nBUA and Ct.vBMD in bovine bone measured *ex vivo* ($R^2 = 0.57$, $p < 10^{-5}$, RMSE = 1.6). These authors also reported the linear fit equation between Ct.nBUA and Ct.vBMD (Ct.nBUA $= -25.2 \times$ Ct.vBMD $+ 40.6$) which can be compared to our result (Ct.nBUA $= -34.1 \times$ Ct.vBMD $+ 45.6$). The differences between these equations may in part be due to the Ct.vBMD range which was different in the two studies: [1.15–1.65] g.cm^{-3} in Sasso *et al* (2008) compared [1.05–1.22] g.cm^{-3} in the present study.

Quality factor Q_{11}^{-1} (table 1) values associated to the propagation of a longitudinal wave can be compared to the shear mode quality factor Q_{44}^{-1} measured from the first resonance peak (falling in the range [100–300 kHz]) of a cuboid bone specimen (Bernard *et al* 2015). In the latter study, the average Q_{44}^{-1} was 3.5% to be compared to a mean value of 8.6% in the present study. These values compare well although the comparison should be made with caution because (i) Q_{44}^{-1} was obtained at a much lower frequency (one order of magnitude); (ii) the

polarization is different and a larger attenuation is expected for shear waves; (iii) the collection of samples used in Bernard *et al* (2015) includes low density (high porosity) samples which may not be representative of the bone of healthy volunteers in the present study.

Ct.nBUA was calculated from measured ultrasound parameters and a value of Ct.Th obtained from the HR-pQCT image of each subject. If only ultrasound data is available, the quality factor Q_{11}^{-1} can be calculated as it does not depend on the bulk wave velocity (equation (9)). Our results suggest that Q_{11}^{-1} could be of clinical interest as it is correlated with Ct.vBMD ($R^2 = 0.92$, figure 4). Furthermore, Fan *et al* (2021) have shown that the shear wave quality factor is correlated to porosity ($R^2 = 0.53$), and it is reasonable to infer that Q_{11}^{-1} measured in this study is also related to porosity.

Signal parameters were estimated in the ultrasound signal with OMP, which has several advantages. The segmentation of the two echoes in the time domain was performed automatically in a robust manner, which can be an advantage in the case of overlapping of echoes (which can occur for thin cortices). Also, because the Gabor function offers a reliable parametrization of the echoes, the calculation of Fourier domain parameters is done avoiding a Fourier transform of the signal which can be polluted by the choice of the time window for time segmentation.

The parametric method used to estimate attenuation relies on the measurement of Δf. In equation (7), β is written in terms of temporal and frequency shifts divided by their associated standard deviations, leading to normalized shifts or Z-scores. Using equations (8), ${Q_{11}}^{-1}$ can also be written in terms of these ratios as $\frac{\Delta f}{\sigma_f} = \frac{1}{2}{Q_{11}}^{-1}\frac{\Delta t}{\sigma_t}$. As the ratio $\Delta t/\sigma_t$ is of the order of 1 and Q_{11}^{-1} is small compared to 1, one can expect the ratio $\Delta f/\sigma_f$ to be also small compared to 1 in accordance with the weak attenuation hypothesis. Thus, special attention should be paid to the evaluation of Δf. Indeed, it can be observed in table 1 that the largest relative uncertainties, up to 70%, are obtained for the frequency Δf parameter, while the uncertainties on the temporal Δt parameter are about a few percent. This observation should be taken into account in order to propose a robust clinical measurement.

The calculation of Ct.nBUA requires the knowledge of Ct.Th, which was obtained from HR-pQCT in the present proof-of-concept study. Our method to measure attenuation could however be implemented together with other ultrasound sequences and signal processing providing speed of sound and Ct.Th as described in Renaud *et al* (2018) or Nguyen Minh (2020).

This study has a number of limitations. (1) Only 5 healthy subjects were considered. The range of cortical bone properties (thickness, material properties) may not be representative of the general population or subjects with bone pathologies. (2) The endosteal interface of cortical bone of young healthy subjects is known to be quasi-plane and regular, whereas it is likely to be irregular and discontinuous for elderly subjects or patients with bone diseases as a result of age- or disease-related bone deterioration and trabecularization (Zebaze *et al* 2010). Such irregular interface may give rise to a wave pattern more complex than the specular echo observed in the young subjects in the present study. Also, as the attenuation is expected to increase with porosity, the signal from the endosteal interface in osteoporostic or old patients should be weaker compared to the signals processed in this study. The applicability of our method to assess aged or diseased bone remains to be assessed. (3) Because the probe was handheld, some pulse-echo acquisitions had to be discarded. We used a quality criterion provided by OMP processing based on the value of the scalar product between the recorded signal and the dictionary. This criterion is believed to be robust as it relies on the expected shape of the echo waveform. Nevertheless, the reproducibility of the method should be assessed in future studies on a larger number of subjects. Moreover, all measurements have been carried out at the same center frequency of 3.5 MHz. This frequency may need to be adapted for smaller or larger thicknesses in order to remain with an endosteal echo clearly separated and not too much attenuated. As attenuation in cortical bone may have a nonlinear dependence on frequency (Yousefian *et al* 2021), attenuation values obtained at different frequencies may not be directly compared with the values obtained in the present study.

The results of this study suggest that ultrasonic quantities (Ct.nBUA and Q_{11}^{-1}) related to attenuation in cortical bone can be measured *in vivo* at the radius, which provides an information on bone quality as they were found to be highly correlated to Ct.vBMD values. Indeed, Ct.vBMD is an established biomarker of bone health related to bone porosity and mineralization (Engelke 2017). If these results are confirmed in studies with a larger number and diversity of subjects, measurement of attenuation may be considered useful for assessing bone health. This can be combined with the measurement of Ct.Th, porosity, and bulk wave velocities in multimodal cortical bone QUS evaluation methods. Future studies should investigate to which extent Ct.nBUA and Q_{11}^{-1} measured with the method of this study reflect the true (intrinsic) ultrasonic attenuation in cortical bone. Advanced signal processing techniques such as neural networks (Mohanty *et al* 2019), machine learning (Minonzio *et al* 2020), or deep learning (Li *et al* 2021) will be investigated in order to improve the robustness of the approach.

Acknowledgments

This work was supported by the GEP scholarship granted by the Guangzhou scholar and ANID ECOS200061 exchange programs. Jean-Gabriel Minonzio is supported by Grant ANID/FONDECYT/REGULAR / 1201311. The authors would like to thank Sylvie Fernandez and Christine Chappard (University Denis Diderot, CNRS, Osteo-Articular Bioengineering and Bioimaging (B2OA) 10, Avenue de Verdun, 75 010 Paris, France) for the HR-pQCT measurements.

Appendix. Orthogonal matching pursuit

A.1. Dictionary

To implement the sparse signal processing method, the first issue is to discretize the Gabor functions into an over-complete dictionary $\mathbf{D}$, where the columns of $\mathbf{D}$ are built resorting to the Gabor functions basis

$$\mathbf{d}(t, \mathbf{\Theta}) = \zeta_{\mathbf{\Theta}} \exp[-s(t-\tau)^2]\exp[j2\pi f(t-\tau)] \tag{A.1}$$

$$\mathbf{\Theta} = [s, \tau, f], \tag{A.2}$$

where $\zeta_{\mathbf{\Theta}}$ is a normalization parameter that ensures $\|\mathbf{d}(\mathbf{\Theta}, t)\|_2 = 1$ (l_2-norm). To build a suitable elementary atom of $\mathbf{D}$, the columns use a discretization of the different parameters that characterize each Gabor function. The possible values of the set of parameters $\mathbf{\Theta}$ are sampled on M discrete points. For this purpose, we define an *a priori* range for s, τ, and f, these ranges being subdivided into L, S and K regular intervals, respectively. Furthermore, each Gabor function is sampled at N_t discrete time points $\mathbf{t} = [t_1, t_2, \cdots, t_{N_t}]$. The dimension of the over-complete dictionary is $M = L \times S \times K$, with $M \gg N_t$. The dictionary can be represented as

$$\mathbf{D} = \begin{bmatrix} d(t_1, \Theta_1) & d(t_1, \Theta_2) & \cdots & d(t_1, \Theta_M) \\ d(t_2, \Theta_1) & d(t_2, \Theta_2) & \cdots & d(t_2, \Theta_M) \\ \vdots & \vdots & \ddots & \vdots \\ d(t_{N_t}, \Theta_1) & d(t_{N_t}, \Theta_2) & \cdots & d(t_{N_t}, \Theta_M) \end{bmatrix}, \tag{A.3}$$

where

$$\Theta_m = [s_l, \tau_s, f_k],$$
$$l \in [1, L],\ s \in [1, S],\ k \in [1, K],\ m \in [1, M].$$

The ranges of variations of s, τ and k are defined as follows. The range of frequency f can be obtained from the bandwidth of the received signal, as discussed in Mor *et al* (2010). Similarly, the range for the bandwidth factor s can be deduced from the bandwidth of the emitted signal. The time delays τ of the different echoes are searched around the peaks of the envelope of the received signal. Overall, the selection of the parameter intervals is quite flexible due to the robustness and efficiency of the OMP method. Using the dictionary, the signal model (1) can be represented as

$$\mathbf{y} = \mathbf{D}\mathbf{x} + \mathbf{n}, \tag{A.4}$$

where $\mathbf{y}$ and $\mathbf{n}$ are the sampling of $y(t)$ and $n(t)$ at discrete time points respectively, $\mathbf{x}$ is the amplitude vector corresponding to each column in $\mathbf{D}$.

This dictionary can be interpreted as an extension of the classical Fourier transform. In the case of the temporal Fourier transform, Θ is reduced to the frequency f and a element of the dictionary matrix writes as $d(t, \Theta) = d(t, f) = \exp(-j2\pi ft)$ and previous equation, i.e. the signal reconstruction, corresponds to the inverse Fourier transform. In case of the Gabor basis, the reconstruction is sparse, i.e. only a finite number of functions are necessary for reconstruction, contrary to the Fourier basis for which the reconstruction is continuous.

We evaluated the numerical cost of the OMP algorithm. For a dictionary size varying from $1000 \times 50\,000$ ($N_t = 1000$; $L = 20$, $K = 10$, $S = 250$) to $1000 \times 80\,000$ ($N_t = 1000$; $L = 20$, $K = 10$, $S = 400$), the computation time ranges approximately between 0.2 and 0.7 s on a standard personal computer (Intel(R) Xeon (R) CPU E5-2620 v2 at 2.10 GHz, 32Gbytes memory, Dell, USA).

A.2. OMP with a complex dictionary

The application considered in this paper is the reconstruction the echoes from the periosteal and endosteal surfaces of the cortical bone. Accordingly, we restrain our analysis to the two first echoes, thus we set $P = 2$ in (1). As a consequence, we expect only 2 non-zero components of $\mathbf{x}$, which is much smaller than its dimension (M). The determination of the two main echoes requires only two iterations using sparsity constrained OMP. Since the columns of the dictionary defined in (3) are complex-valued, the corresponding steps of the OMP have

to be adapted. Each iteration step consists in searching the best matching column with the residual from the previous iteration. In the case of a complex dictionary, the matching between a particular complex column and the given signal r is (Lu and Michaels 2008)

$$\langle \mathbf{r},\, \mathbf{d}^H \rangle = \mathbf{d}^H \mathbf{r} = Ce^{j\phi}, \tag{A.5}$$

where $\mathbf{r}$ is the residual signal from the last iteration, H denotes the complex conjugate transpose operator, C indicates the matching level, and ϕ the phase of the residual.

The best-correlated column from the dictionary $\mathbf{D}$ corresponds to the largest value of C. The corresponding position index in vector $\mathbf{x}$ is denoted

$$i_{\max} = \max_i \{|\mathbf{D}(:,i)^H \mathbf{r}|\}, \tag{A.6}$$

and the phase is given by

$$\phi = \text{angle}\{\mathbf{D}(:,i_{\max})^H\, \mathbf{r}\}. \tag{A.7}$$

It should be noticed that the residual cannot be iterated directly, since it is defined as the linear combination of two real Gaussian pulses instead of complex-values Gabor functions as introduced in (A.1). After computation of (A.6) and (A.7), The real Gaussian pulses $\mathbf{D}_r(i_{\max})$ are obtained using the relationship

$$\mathbf{D}_r(:,\ i_{\max}) = \Re\{\mathbf{D}(:,\ i_{\max}) e^{-j\phi}\}. \tag{A.8}$$

The OMP processing is illustrated in algorithm 1.

Algorithm 1. Orthogonal matching pursuit algorithm.

Input: $\mathbf{y} \in \mathbb{R}^N$, $\mathbf{D} \in \mathbb{C}^{N\times M}$, target sparsity=2
Output: sparse solution $\mathbf{x} \in \mathbb{R}^M$
1: Set $I = ()$, $\mathbf{r} = \mathbf{y}$, $\mathbf{D}_r = \mathbf{D}(:,\ I)$
2: **for** target sparsity **do**
3: $i_{\max} = \max_i |\mathbf{D}(:,\ i)^H \mathbf{r}|$
4: $\mathbf{I} = (\mathbf{I},\ \mathbf{i}_{\max})$
5: $\phi = \text{angle}\{\mathbf{D}(:,i_{\max})^H\, \mathbf{r}\}$
6: $\mathbf{D}_r(:,\ i_{\max}) = \Re\{\mathbf{D}(:,\ i_{\max}) e^{-j\phi}\}$
7: $\mathbf{x}(I) = \mathbf{D}_r(:,\ I)^\dagger \mathbf{y}$ †denotes pseudo inverse
8: $\mathbf{r} = \mathbf{y} - \mathbf{D}_r(:,\ I)\mathbf{x}(I)$
9: **end for**

ORCID iDs

Jean-Gabriel Minonzio https://orcid.org/0000-0003-1364-0560
Didier Cassereau https://orcid.org/0000-0003-2412-2144
Quentin Grimal https://orcid.org/0000-0001-9041-8176

References

Bala Y *et al* 2014 Cortical porosity identifies women with osteopenia at increased risk for forearm fractures *J. Bone Miner. Res.* **29** 1356–62
Bernard S, Schneider J, Varga P, Laugier P, Raum K and Grimal Q 2015 Elasticity-density and viscoelasticity-density relationships at the tibia mid-diaphysis assessed from resonant ultrasound spectroscopy measurements *Biomech. Model. Mechanobiol.* **15** 97–109
Boutroy S, Bouxsein M L, Munoz F and Delmas P D 2005 *In vivo* assessment of trabecular bone microarchitecture by high-resolution peripheral quantitative computed tomography *J. Clin. Endocrinol. Metab.* **90** 6508–15
Briot K, Paternotte S, Kolta S, Eastell R, Felsenberg D, Reid D M, Glüer C C and Roux C 2013 FRAX®: Prediction of major osteoporotic fractures in women from the general population: the OPUS study *PLoS One* **8** e83436
Choksi P, Jepsen K J and Clines G A 2018 The challenges of diagnosing osteoporosis and the limitations of currently available tools *Clin. Diabetes Endocrinol.* **4** 12
Demirli R and Saniie J 2001 Model-based estimation of ultrasonic echoes: II. Nondestructive evaluation applications *IEEE Trans. Ultrason. Ferroelectr. Freq. Control* **48** 803–11
Dencks S, Barkmann R, Padilla F, Laugier P, Schmitz G and Gluer C C 2008 Model-based estimation of quantitative ultrasound variables at the proximal femur *IEEE Trans. Ultrason. Ferroelectr. Freq. Control* **55** 1304–15
Engelke K 2017 Quantitative computed tomography current status and new developments *J. Clin. Densitometry* **20** 309–21
Fan F, Cai X, Follet H, Peyrin F, Laugier P, Niu H and Grimal Q 2021 Cortical bone viscoelastic damping assessed with resonant ultrasound spectroscopy reflects porosity and mineral content *J. Mech. Behav. Biomed. Mater.* **117** 104388
Foiret J, Minonzio J G, Chappard C, Talmant M and Laugier P 2014 Combined estimation of thickness and velocities using ultrasound guided waves: a pioneering study on *in vitro* cortical bone samples *IEEE Trans. Ultrason. Ferroelectr. Freq. Control* **61** 1478–88

Grimal Q and Laugier P 2019 Quantitative ultrasound assessment of cortical bone properties beyond bone mineral density *IRBM* **40** 16–24
Han S, Rho J, Medige J and Ziv1 I 1996 Ultrasound velocity and broadband attenuation over a wide range of bone mineral density *Osteoporosis Int.* **6** 291–6
Holzer G, von Skrbensky G, Holzer L A and Pichl W 2009 Hip fractures and the contribution of cortical versus trabecular bone to femoral neck strength *J. Bone Miner. Res.* **24** 468–74
Iori G, Du J, Hackenbeck J, Kilappa V and Raum K 2020 Estimation of cortical bone microstructure from ultrasound backscatter *IEEE Trans. Ultrason. Ferroelectr. Freq. Control* **68** 1081–95
Karjalainen J, Riekkinen O, Toyras J, Kroger H and Jurvelin J 2008 Ultrasonic assessment of cortical bone thickness *in vitro* and *in vivo IEEE Trans. Ultrason. Ferroelectr. Freq. Control* **55** 2191–7
Kral R, Osima M, Borgen T T, Vestgaard R, Richardsen E and Bjørnerem Å 2017 Increased cortical porosity and reduced cortical thickness of the proximal femur are associated with nonvertebral fracture independent of fracture risk assessment tool and garvan estimates in postmenopausal women *PLos One* **12** e0185363
Kuc R 1984 Estimating acoustic attenuation from reflected ultrasound signals: comparison of spectral-shift and spectral-difference approaches *IEEE Trans. Ultrason. Ferroelectr. Freq. Control* **32** 1–6
Kuc R, Schwartz M and Micsky L V 1976 Parametric estimation of the acoustic attenuation coefficient slope for soft tissue *1976 Ultrasonics Symposium (Annapolis, MD, 29 September–1 October 1976)* (Piscataway, NJ: IEEE) pp 44–7
Laib A, Häuselmann H and Rüegsegger P 1998 *In vivo* high resolution 3D-QCT of the human forearm *Technol. Health Care* **6** 329–37
Lakes R, Yoon H S and Katz J L 1986 Ultrasonic wave propagation and attenuation in wet bone *J. Biomed. Eng.* **8** 143–8
Langton C M and Njeh C F 2008 The measurement of broadband ultrasonic attenuation in cancellous bone-a review of the science and technology *IEEE Trans. Ultrason. Ferroelectr. Freq. Control* **55** 1546–54
Lees S and Klopholz D Z 1992 Sonic velocity and attenuation in wet compact cow femur for the frequency range 5 to 100 MHz *Ultrasound Med. Biol.* **18** 303–8
Li Y, Xu K, Li Y, Xu F, Ta D and Wang W 2021 Deep learning analysis of ultrasonic guided waves for cortical bone characterization *IEEE Trans. Ultrason. Ferroelectr. Freq. Control* **68** 935–51
Lu Y and Michaels J E 2008 Numerical implementation of matching pursuit for the analysis of complex ultrasonic signals *IEEE Trans. Ultrason. Ferroelectr. Freq. Control* **55** 173–82
MacNeil J A and Boyd S K 2007 Accuracy of high-resolution peripheral quantitative computed tomography for measurement of bone quality *Med. Eng. Phys.* **29** 1096–105
Mamou J and Oelze M L 2013 *Quantitative Ultrasound in Soft Tissues* (Berlin: Springer) (https://doi.org/10.1007/978-94-007-6952-6)
Minonzio J G, Bochud N, Vallet Q, Ramiandrisoa D, Etcheto A, Briot K, Kolta S, Roux C and Laugier P 2019 Ultrasound-based estimates of cortical bone thickness and porosity are associated with nontraumatic fractures in postmenopausal women: a pilot study *J. Bone Miner. Res.* **34** 1585–96
Minonzio J G, Cataldo B, Olivares R, Ramiandrisoa D, Soto R, Crawford B, De Albuquerque V H C and Munoz R 2020 Automatic classifying of patients with non-traumatic fractures based on ultrasonic guided wave spectrum image using a dynamic support vector machine *IEEE Access* **8** 194752–64
Minonzio J G, Foiret J, Talmant M and Laugier P 2011 Impact of attenuation on guided mode wavenumber measurement in axial transmission on bone mimicking plates *J. Acoust. Soc. Am.* **130** 3574–82
Mohanty K, Yousefian O, Karbalaeisadegh Y, Ulrich M, Grimal Q and Muller M 2019 Artificial neural network to estimate micro-architectural properties of cortical bone using ultrasonic attenuation: a 2-d numerical study *Comput. Biol. Med.* **114** 103457
Moilanen P 2008 Ultrasonic guided waves in bone *IEEE Trans. Ultrason. Ferroelectr. Freq. Control* **55** 1277–86
Mor E, Azoulay A and Aladjem M 2010 A matching pursuit method for approximating overlapping ultrasonic echoes *IEEE Trans. Ultrason. Ferroelectr. Freq. Control* **57** 1996–2004
Narayana P A and Ophir J 1983 On the validity of the linear approximation in the parametric measurement of attenuation in tissues *Ultrasound Med. Biol.* **9** 357–61
Nguyen Minh H, Du J and Raum K 2020 Estimation of thickness and speed of sound in cortical bone using multifocus pulse-echo ultrasound *IEEE Trans. Ultrason. Ferroelectr. Freq. Control* **67** 568–79
Nishiyama K K, Macdonald H M, Buie H R, Hanley D A and Boyd S K 2010 Postmenopausal women with osteopenia have higher cortical porosity and thinner cortices at the distal radius and tibia than women with normal aBMD: an *In Vivo* HR-pQCT Study *J. Bone Miner. Res.* **25** 882–90
Ostertag A, Peyrin F, Gouttenoire P J, Laredo J, DeVernejoul M, Cohen-Solal M and Chappard C 2016 Multiscale and multimodality computed tomography for cortical bone analysis *Phys. Med. Biol.* **61** 8553–76
Paranhos-Neto F *et al* 2019 Vitamin d deficiency is associated with cortical bone loss and fractures in the elderly *Eur. J. Endocrinol.* **181** 509–17
Renaud G, Clouzet P, Cassereau D and Talmant M 2020 Measuring anisotropy of elastic wave velocity with ultrasound imaging and an autofocus method—application to cortical bone *Phys. Med. Biol.* **65** 235016
Renaud G, Kruizinga P, Cassereau D and Laugier P 2018 *In vivo* ultrasound imaging of the bone cortex *Phys. Med. Biol.* **63** 125010
Sai H *et al* 2010 Novel ultrasonic bone densitometry based on two longitudinal waves: significant correlation with pQCT measurement values and age-related changes in trabecular bone density, cortical thickness, and elastic modulus of trabecular bone in a normal Japanese population *Osteoporosis Int.* **21** 1781–90
Sasso M, Haïat G, Yamato Y, Naili S and Matsukawa M 2008 Dependence of ultrasonic attenuation on bone mass and microstructure in bovine cortical bone *J. Biomech.* **41** 347–55
Siris E 2004 Absolute versus relative fracture risk *J. Bone Miner. Res.* **20** 705–705
Szabo T L 1995 Causal theories and data for acoustic attenuation obeying a frequency power law *J. Acoust. Soc. Am.* **97** 14–24
Talmant M, Renaud G and Grimal Q 2019 Measurement of ultrasonic anisotropic attenuation of P-wave in millimeter-sized human cortical bone samples *8th Int. Symp. on Ultrasonic Characterization of Bone (Fréjus, France, June 24-26)*
Tropp J A and Gilbert A C 2007 Signal recovery from random measurements via orthogonal matching pursuit *IEEE Trans. Inf. Theory* **53** 4655–66
Yousefian O, Karbalaeisadegh Y and Muller M 2021 Frequency-dependent analysis of ultrasound apparent absorption coefficient in multiple scattering porous media: application to cortical bone *Phys. Med. Biol.* **66** 035026
Yousefian O, White R D, Karbalaeisadegh Y, Banks H T and Muller M 2018 The effect of pore size and density on ultrasonic attenuation in porous structures with mono-disperse random pore distribution: a two-dimensional in-silico study *J. Acoust. Soc. Am.* **144** 709–19
Zebaze R M, Ghasem-Zadeh A, Bohte A, Iuliano-Burns S, Mirams M, Price R I, Mackie E J and Seeman E 2010 Intracortical remodelling and porosity in the distal radius and post-mortem femurs of women: a cross-sectional study *Lancet* **375** 1729–36

Zheng R, Le L H, Sacchi M D and Lou E 2009 Broadband ultrasound attenuation measurement of long bone using peak frequency of the echoes *IEEE Trans. Ultrason. Ferroelectr. Freq. Control* **56** 396–9
Zheng R, Le L H, Sacchi M D, Ta D and Lou E 2007 Spectral ratio method to estimate broadband ultrasound attenuation of cortical bones in vitrousing multiple reflections *Phys. Med. Biol.* **52** 5855–69